PERGAMON

Vision Research 41 (2001) 2057–2064

Vision Research

www.elsevier.com/locate/visres

Neural synergy in visual grouping: when good continuation meets common fate

Sang-Hun Lee, Randolph Blake *

Vanderbilt Vision Research Center, Vanderbilt University, 111 21st Avenue S., Nashville, TN 37240, USA

Received 30 October 2000; received in revised form 12 February 2001

Abstract

A modified version of the 'path finder' display consisting of many small oriented Gabor patches was used to study the joint contributions of spatial and temporal structures to shape perception. A two-interval forced-choice procedure measured detectability of curved 'paths' defined by orientation ('good continuation') and/or by temporal synchrony of change in motion direction ('common fate'). When orientation was completely random (no spatial 'path' cue) temporal synchrony still supported reliable performance, but only when correlation of change among 'path' elements was high. When combined, these two weak spatial and temporal structures yielded performance in excess of probability summation: 'paths' weakly defined by orientation were highly conspicuous when the constituent Gabors underwent synchronized changes in direction of motion, even though the individual directions of path elements were uncorrelated. Spatial grouping from temporal structure may arise from correlated transients associated with synchronized changes in motion direction. Evidently these two mechanisms for promotion of spatial grouping interact synergistically.

Keywords: Contours; Visual grouping; Spatial structure; Temporal structure

1. Introduction

Last century the Gestalt psychologists identified several important principles of visual perceptual grouping, including common fate and good continuation (Koffka, 1935). Good continuation, a spatial organizing principle, states that neighboring visual features tend to group together forming an extended contour when those features are spatially aligned. Common fate, a temporal organizing principle, states that visual elements moving in the same general direction at the same speed tend to be grouped into a single global object. In recent years refined examples of the operation of these two principles have been developed (e.g. Regan & Hamstra, 1992; Field, Hayes, & Hess, 1993), and possible neural instantiations of these principles have been proposed (e.g. Gilbert, 1993; Lamme, 1995). These recent developments now set the stage for asking how spatial and temporal structure interact jointly to specify visual shapes and to support figure/ground segmentation (Fahle & Koch, 1995; Kiper, Gegenfurtuer, & Movshon, 1996; Alais, Blake, & Lee, 1998; Usher & Donnelly, 1998; Roelfsema, Scholte, & Spekreijse, 1999; Gepshtein & Kubory, 2000). In this report we show that common fate and good continuation synergistically interact to specify the presence of an object within a cluttered background. These results are novel in that they utilize stochastic temporal events to define 'common fate'.

We utilized the so-called 'path-finder' displays (Fig. 1b) first devised by Beck (1983) and subsequently refined by others (Grossberg & Mingolla, 1985; Kellman & Shipley, 1991; Kovacs & Julesz, 1993; Field et al., 1993). These displays consist of an array of irregularly spaced contours whose orientations are randomized except for a small subset of neighboring 'target' contours whose orientations are aligned to create a smoothly curved 'path'. The orientation of each 'target' contour, however, can deviate, within a given range, from the orientation defined by the path (the value α in Fig. 1a). As the range of possible angular deviations increases, the 'path' becomes more difficult to detect

* Corresponding author. Tel.: +1-615-3437010; fax: +1-615-3435027.

E-mail address: randolph.blake@vanderbilt.edu (R. Blake).

0042-6989/01/$ - see front matter
PII: S0042-6989(01)00086-4

because the spatial property promoting 'good continuation' is degraded. To implement common fate within these path-finder displays, we made the contours within each stationary patch move in one of two directions orthogonal to their orientation, with the direction of motion reversing irregularly over time. Points in time at which reversals occurred were uncorrelated among 'background' elements but were correlated to varying degrees among the nine 'target' elements defining the path (the value r in Fig. 1c). In addition, the contrast of each element was randomly set; this irregularity in contrast throughout the display precluded creation of extraneous cues from temporal integration (Adelson & Farid, 1999; Lee & Blake, 1999b). Using a two interval, forced-choice procedure we measured path detectability for different values of spatial structure (α) and different levels of temporal structure (r). It is important to note that the directions of motion of individual 'path' elements were completely uncorrelated and, therefore, motion grouping provided no clue about the location of the path.

2. Methods

2.1. Apparatus

All gray-scale animations were displayed on a NEC 21-inch RGB monitor (frame rate 100 Hz; pixel resolution 1024×768; P104 phosphor) under low ambient illumination using MatLab© in conjunction with the Psychophysics toolbox (Brainard, 1997). Luminance nonlinearities were corrected using a look-up table resulting in 184 gray levels. The mean luminance of the screen was 24.5 cd/m^2.

2.2. Stimuli

Each animation frame consisted of 121 small oriented Gabor patches distributed within an 11×11 element array subtending 5.5×5.5 deg of visual angle. The peak spatial frequency of every grating was 3.8 cycles per degree, filtered by a circular Gaussian envelope with a S.D. of 6 arc min. Half of the displays contained a 'path', shown as a bold line in Fig. 1a, consisted of nine virtual line segments which were correlated in terms of relative orientation. The length of these virtual segments (D) was varied ($\Delta D = \pm 0.02$ deg) around 0.14 degree to make sure that the density of the elements in the path are equated with the density of the background elements. The curvature of the path was determined by the angular difference among neighboring segments ($\beta = 30$ deg, $\Delta\beta = \pm 5$ deg). Placed at the midpoint of each virtual segment was a Gabor patch, and the orientation of each Gabor deviated from the orientation of its corresponding path segment by an amount that varied over trials. The range of the angular deviations (α) was systematically varied from ± 10 to ± 90 deg. In the '± 90 deg' condition, for instance, the size of angular deviation in each path element was randomly selected from the uniform distribution with the range from -90 to $+90$ deg. After the locations and orientations of the path elements were determined, the background elements were distributed over the 112

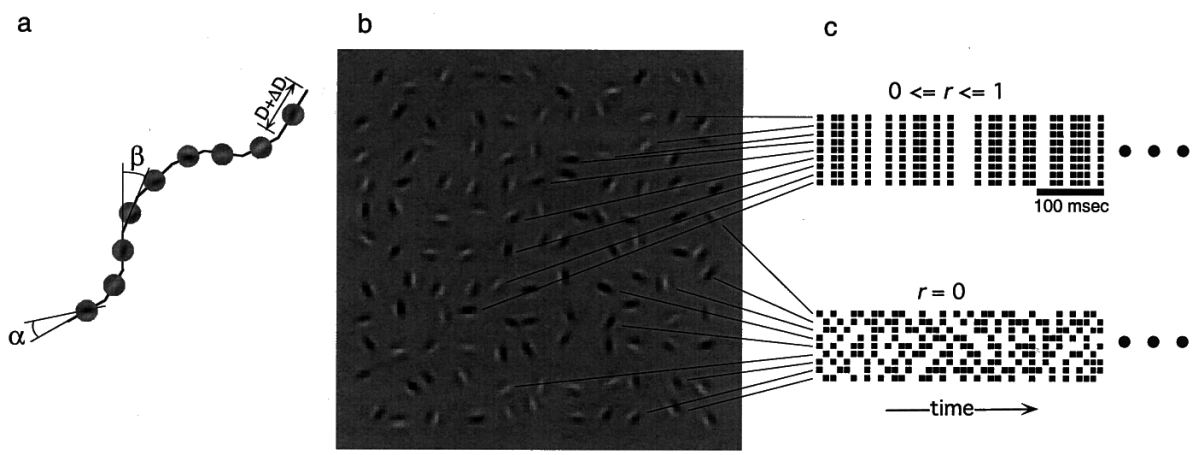

Fig. 1. An example of the displays used in this study. (a) The 'target' path, shown as a bold line, consisted of nine virtual line segments. The length D is the length of virtual segment on which a Gabor patch was placed. The angular difference among neighboring segments determined the overall curvature of the path. The range of the angular deviations (α) was systematically varied in the experiments. (b) One example of a display containing a 'path' composed of nine target Gabors appearing within an array of 'background' Gabors whose orientations are random. (c) Temporal structure of individual elements was defined by irregular changes in direction of motion (in the first experiment) or in luminance contrast (the second experiment). The series of small dots denote for all nine target elements and a couple of background elements the points in time at which these changes occured. Average correlation in temporal structure (r) was always zero among background elements and varied from zero to unity among target elements.

square grids that were not occupied by the path elements. The orientation of each background element was randomly determined and its location was randomly jittered within a given square grid. Images for all animations used in one block of experiment were made and stored on the computer before each block of experiment.

2.3. Experimental procedures

In both experiments a two-interval forced-choice (2IFC) procedure was used to measure detectability of the path. On each trial two successive displays were sequentially presented each for 1 s, with a 0.5 s interval between. One interval contained randomly oriented Gabor patches only (no path) and the other interval contained the nine aligned target elements defining the path plus 112 'background' elements. The shape and location of the 'path' within the entire array varied randomly over trials. On each trial observers fixated the center of the array and reported in which interval the 'path' appeared, guessing if necessary. Feedback was given following each trial.

In the first experiment, the contours within each stationary Gabor patch moved at 5.2 degree per second in one of two directions orthogonal to their orientation by phase-shifting the grating from frame to frame of the animation by one-fifth of the grating cycle at every 10 ms; the starting phases of the gratings were random. The contrast of all gratings was randomized within the range 0.4–0.8 throughout the display to preclude extraneous cues from temporal integration (Adelson & Farid, 1999; Lee & Blake, 1999b). Temporal structure of individual elements was defined by irregular changes in direction of motion. The series of small dots in Fig. 1c denote, for all nine target elements and a sample of background elements, the points in time at which motion direction changed — each series of dots constitutes what can be termed a 'point process' (i.e. a history of the points in time at which change occurred). Temporal structure was created by randomly deciding direction of motion (probability of motion in each direction was 0.5) every animation frame (i.e. every l0 ms, given the monitor's 100 Hz refresh rate) with the constraint that no more than three consecutive 'change' frames or more than three consecutive 'no change' frames were allowed. These restrictions, in conjunction with contrast randomization, were introduced to remove potential extraneous cues associated with temporal integration (Lee & Blake, 1999b). Average correlation in temporal structure was always zero among the background elements ($r = 0$) and varied from zero to unity ($r = 1$, as illustrated in the figure) among the nine path elements. On each trial, the average correlation in temporal structure among the target elements comprising the 'path' was one of five values (0, 0.25, 0.5, 0.75 or 1), with the particular value varying randomly over trials. 'Average correlation' was computed by averaging correlations between all possible pairs of point processes for the target elements (i.e. the average of 36 pairs of correlations for the nine target elements). To produce a group of point processes with a specific average correlation value, we used a following algorithm. First, a 'seed' point process was generated. Nine point processes associated with target elements were generated by shuffling (switching positions between randomly selected points) the 'seed' point process a certain number of times (depending on a given average correlation value). This shuffling procedure was repeated until the average correlation among those newly generated point processes fell within a narrow range around the desired correlation value (e.g. 0.5 ± 0.01).

In the second experiment gratings were stationary and the contrast of the gratings alternated unpredictably over time between two given values. The mean contrast of each grating was randomly set to a value within the range 0.25–0.5, and the contrast of each grating was modulated by ± 0.24 log-units about its mean value. The average correlation in temporal structure (the series of time points at which contrast changed) among the target elements comprising the 'path' was one of three values — 0, 0.5, or 1 — with the particular value varying randomly over trials.

Each block of trials consisted of 25 (in experiment 1) or 15 (in experiment 2) conditions (as all possible combinations of 'five different ranges of the angular deviations (α) of the path elements' and 'five (in experiment 1) or three (in experiment 2) different levels of temporal correlation (r) among the path elements') with ten trials in each condition. Each block was repeated 12 times on different days (two or three blocks on each day) resulting in a total of 120 trials in each condition.

2.4. Statistics

To test for statistical significance, we used a bootstrapping procedure (Efron & Tibshirani, 1986, 1993) to estimate the threshold and confidence interval associated with a given psychometric function. This procedure consisted of the following steps. Step 1 involved obtaining the best-fit psychometric function to the obtained percent correct values using the cumulative normal curve:

$$p = 0.5 * \left[(2\pi)^{-1/2} \int_{-\infty}^{z} \exp(-u^2/2)\, \mathrm{d}u \right] + 0.5,$$
$$z = (x - t)/\mathrm{sig}, \quad (1)$$

where t and 1/sig specify the threshold and the slope of the curve, respectively. (The value 0.5 was used to rescale the cumulative normal function since the lower asymptote is 0.5 in a 2IFC task.) In Step 2 a bootstrap sample $P^* = \{P_1^*, P_2^*, \ldots, P_m^*\}$ was generated based on

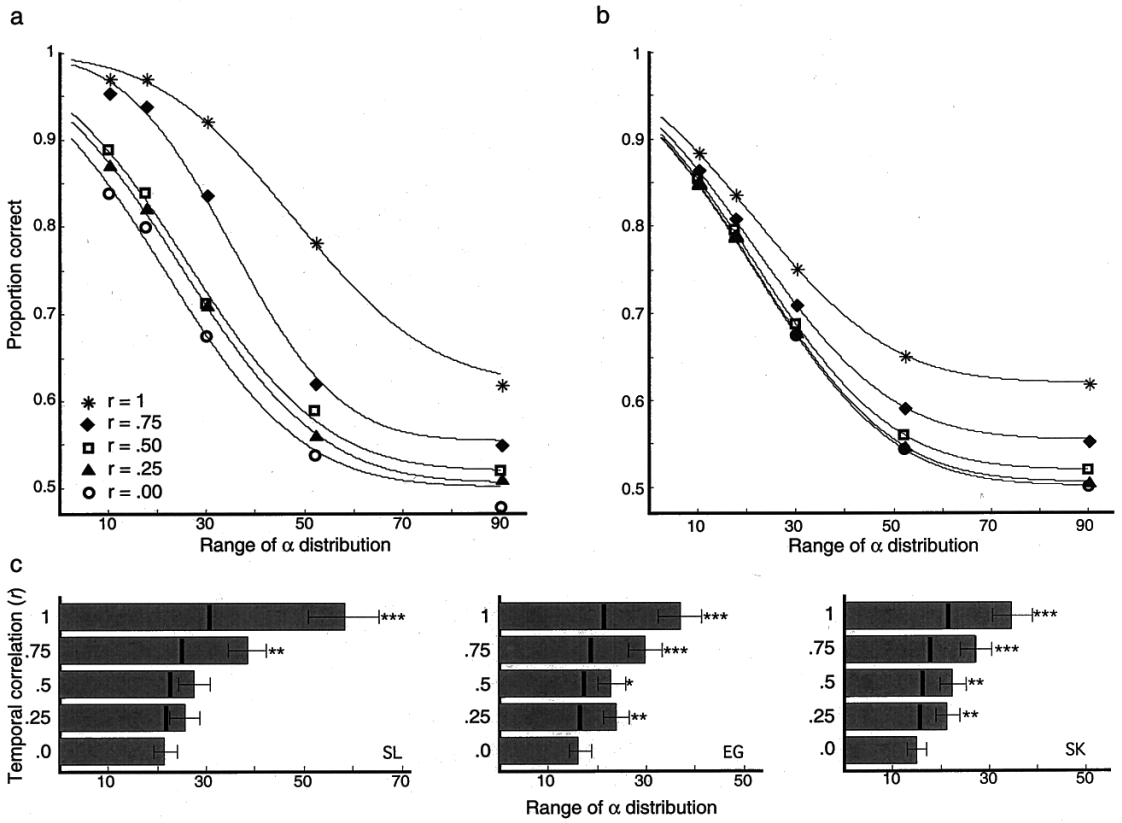

Fig. 2. Results from experiment 1. (a) Proportion-correct performance for observer SL on the path detection task where the range of angular deviation of the target elements relative to the path (α) and the average correlation in temporal structure among the target elements (r) were manipulated. Each data point is based on 120 trials. Solid lines show psychometric functions fit by cumulative normal functions to data sets for each of the five temporal correlation values. (b) Psychometric curves for observer SL predicted from probability summation. (c) For each of the three observers, gray bars represent 75% thresholds estimated from the psychometric functions for each of five values of temporal correlation; error bars represent 68% confidence intervals which were estimated from the 5000 bootstrap samples (see Section 2.4). Thick dark lines indicate threshold values predicted by probability summation. *Confidence interval $>95\%$; **confidence interval $>99.5\%$; ***confidence interval $>99.99\%$.

the assumption that p_i at stimulus x_i is generated from a binomial distribution with the standard error:

$$\sigma_i = \sqrt{p_i*(1-p_i)/n_i}, \tag{2}$$

where n_i is the number of trials at stimulus x_i. In Step 3 the bootstrap sample (P^*) was fitted based on Eq. (1) to estimate a 75% threshold (t^*). Step 1 and step 2 were repeated 5000 times, resulting in 5000 bootstrap estimates of threshold ($t_1^*, t_2^*, \ldots, t_{5000}^*$). In Step 4 the mean of the bootstrap threshold estimates:

$$t = \sum_{b=1}^{5000} t_b^*/5000, \tag{3}$$

was used as the final estimate of the threshold of the psychometric function $P = \{P_1, P_2, \ldots, P_m\}$. In Step 5 the 95% confidence interval of the threshold was determined by finding the 2.5th and 97.5th percentiles of the bootstrap thresholds ($t_1^*, t_2^*, \ldots, t_{5000}^*$) since the actual distribution of t^* may be skewed rather than normal.

2.5. Observers

Four observers, with normal or corrected vision, participated in the experiments. One of them was one of the authors (SL), and the other three observers were unaware of the purpose of the experiments.

3. Results

3.1. Experiment 1

The results are summarized in Fig. 2. As expected path detectability varied with the degree of good continuation, i.e., angular difference in orientation of a target from the path (Field et al., 1993); this was true for all levels of temporal structure. In the absence of correlated temporal structure, the task eventually became impossible when the path targets were completely unconstrained in local orientation (in Fig. 2a, $r = 0$; $\alpha = \pm 90$), which makes sense because global spatial

structure has been destroyed. when these spatially unstructured path targets all shared the same temporal structure ($\alpha = \pm 90$; $r = 1$), however, observers were able to perform the task at above-chance levels (Fig. 2a). In other words, temporal structure alone can promote spatial grouping, as shown in earlier work (Lee & Blake, 1999a). More revealing, however, was performance under conditions where spatial structure was weak but present. Here some degree of common temporal structure among path targets facilitated detection, by an amount greater than that expected on the basis of probability summation estimated from performance levels measured in the absence of spatial structure and in the absence of temporal structure.

To quantitatively evaluate this synergistic interaction between spatial structure and temporal structure, 75% thresholds were estimated from the psychometric functions for different values of temporal correlation (gray bars in Fig. 2c). Then, these values were compared to corresponding thresholds predicted by probability summation values (indicated by dark lines in Fig. 2c). These predictions were derived using two sets of probability values: $P_{\alpha(i)|r=0}$, probability of correct detection across different values of α in the absence of temporal structure, and $P_{r(j)|\alpha=\pm 90}$, the probability of correct detection across different values of temporal correlation in the absence of spatial structure ($\alpha = \pm 90$). Using these values, we derived psychometric curves (Fig. 2b) predicted on the basis of probability summation:

$$P'_{\alpha(i),r(j)} = 1 - (1 - P'_{\alpha(i)|r=0}) * (1 - P'_{r(j)|\alpha=\pm 90}), \quad (4)$$

where $P' = (P - c)/(d - c)$, $d = 1$ and $c = 0.5$ in a 2IFC task, and derived 75% thresholds from these psychometric curves. Thresholds derived from the actual data exceed those predicted from probability summation. To test the statistical significance of these differences, we applied t-tests with the null hypothesis that the measured threshold equals the predicted threshold. We estimated the confidence intervals for the measured thresholds using the parametric bootstrapping procedure (see Section 2.4). In most of the comparisons across observers (10 out of 12), the measured thresholds were significantly higher than the thresholds predicted from probability summation. This enhanced performance in excess of probability summation is a hallmark of neural synergy among multiple sources of visual information (Graham, 1989).

To validate our analytic formulation of probability summation, we performed a control experiment which included a condition in which the interaction between temporal and spatial structure *cannot* exceed that associated with probability summation. In this condition, two separate, independently generated target paths were presented simultaneously, one path defined only by spatial structure and the other defined only by temporal structure. Thus on each trial of this condition, the observer could judge the correct interval based on detection of either of these two independent paths. Performance on this condition should be superior to that measured when only a single path is presented, since the observer has two independent chances to detect. This 'two-path' display thus provides an empirical estimate of the level of performance expected on the basis of probability summation.

The experiment, performed using two observers, consisted of four conditions: (i) a 'spatial path' condition in which a single target path defined only by spatial structure was presented ($\alpha = \pm 35$, $r = 0$ for observer SL, and $\alpha = \pm 20$, $r = 0$ for observer CA); (ii) a 'temporal path' condition in which a single target path defined only by temporal structure was presented ($\alpha = \pm 90$, $r = 1$ for SL and $\alpha = \pm 90$, $r = 1$ for CA); (iii) a 'two-path' condition in which two target paths were presented simultaneously at two different locations, one path defined only by spatial structure ($\alpha = \pm 35$, $r = 0$ for SL and $\alpha = \pm 20$, $r = 0$ for CA) and the other only by temporal structure ($\alpha = \pm 90$, $r = 1$ for SL and $\alpha = \pm 90$, $r = 1$ for CA); (iv) a 'single path' condition in which a single target path defined by both spatial and temporal structure was presented ($\alpha = \pm 35$, $r = 1$ for SL and $\alpha = \pm 20$, $r = 1$ for CA). When generating displays for the 'two-path' condition, we discarded displays in which the two paths shared more than one element because spatial and temporal structure cannot be defined independently when element overlap exceeds one. These four conditions were randomized within a given block of trials.

Fig. 3 shows the results. Once again, the combination of spatial and temporal structure in a single-path display (condition (iv)) yielded a performance significantly better than the probability summation prediction shown by the dotted line ($P < 0.0001$ in SL and $P < 0.01$ in CA). Performance on the two-path condition, however, was not significantly different from that predicted by probability summation ($P > 0.9$ in SL and $P > 0.3$ in CA). This latter finding validates the use of Eq. (4) as an analytic expression of probability summation and further supports our conclusion that spatial and temporal structure are interacting synergistically in these pathfinder displays.

It is known that stationary objects carrying local motion cues (like Gabor elements in our displays) are perceived as being displaced in the direction of motion (De Valois & De Valois, 1991). This implies that perceived locations of local Gabor elements in our displays are jittered over time due to unpredictable changes in motion vectors as recently demonstrated by Hayes (2000). It should be stressed, however, that this effect cannot account for enhanced detectability of paths whose elements shared a common temporal changes in direction of motion since the initial motion directions of local elements in our displays were randomly determined.

3.2. Experiment 2

By definition the orientations of contours defining the 'path' are related to some degree and, of course, their directions of motion are constrained by their orientations. Is it possible, therefore, that observers were utilizing some sense of global motion, not synchronized change in direction, as the temporal cue for grouping? This seems unlikely since neighboring targets differed in orientation, on average, by 30 deg and the specific directions of motion among path targets were always uncorrelated. Still, to ascertain that it was synchronized change that supported grouping, we repeated this experiment now using changes in contrast as the embodiment of temporal structure. Contours within each Gabor patch were stationary, but their contrast values changed irregularly over time according to a Poisson process. Again, the individual contrast values of both 'target' and 'background' elements were randomized throughout the array. The time points for contrast changes were uncorrelated among 'background' elements but were correlated to varying degrees among 'path' elements. It should be stressed that contrast per se provided no cue for grouping, for the variations in contrast for all elements were unrelated in direction and value.

Using contrast modulation as the carrier of temporal structure, we found the same pattern of results (Fig. 4): both observers tested on this condition were able to detect paths at a detection rate in excess of probability summation when the elements defining a path were jointly determined by spatial and temporal information. This result reinforces our conviction that observers were relying on 'change' and not motion per se in our first experiment.

4. Discussion

It has been suggested that the extended path defined by aligned Gabor elements is not detected by a single neural filter (Hess & Dakin, 1997). Instead, it is commonly believed that good continuation in these path-finder displays is more likely to be promoted by long-range lateral connections among orientation-selective neurons in neighboring cortical columns (Kovacs & Julesz, 1993; Field et al., 1993; Grossberg & Mingolla, 1985). Indeed, there is anatomical and physiological evidence for the existence of such connections (Das & Gilbert, 1995; Bosking, Zang, Schofield, & Fitzpatric, 1997; Schmidt, Kim, Singer, Bonhoffer, & Löwel, 1997). According to this evidence, the long-range connections are formed primarily among orientation columns containing neurons exhibiting similar orientation preferences, with the length of those connections being longer among orientation columns that are collinear in orientation preference compared to orientations parallel to one another. These neural properties dovetail with psychophysical findings using path-finder displays (Field et al., 1993).

Given this view of the neural structure underlying 'good continuation' in these displays, our findings imply that fine temporal structure in the optical input to vision can modulate the effective strength of these connections and, hence, the tendency of neighboring figural elements to group into coherent, global shapes. Furthermore, the synergistic interaction between spatial and temporal structure in contour integration suggests that the efficacy of temporal structure in modulating connection strength is constrained by spatial factors including orientation similarity and receptive field

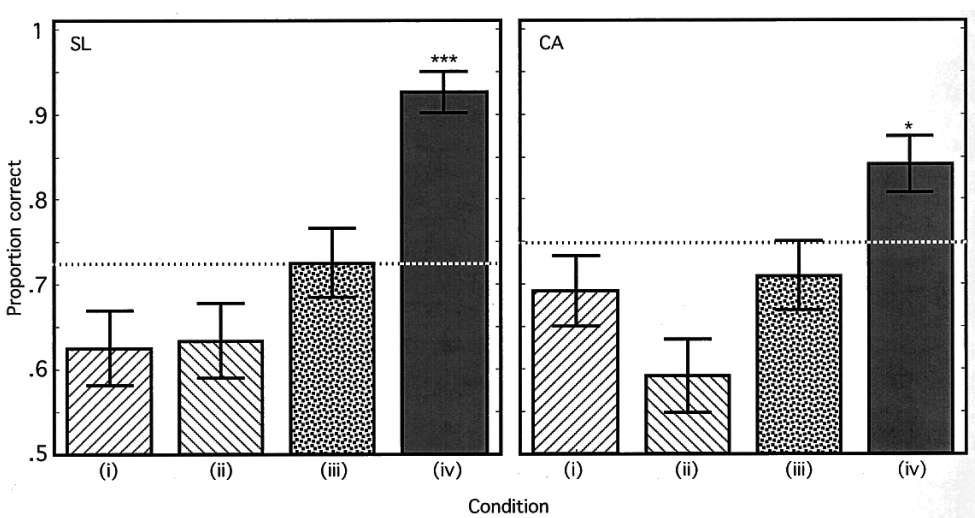

Fig. 3. Proportion-correct performance for two observers, SL and CA, on the path detection task under four conditions: (i) the 'spatial path' condition, (ii) the 'temporal path' condition, (iii) the 'two-path' condition, and (iv) the 'single path' condition. Dotted lines indicate performance predicted from probability summation (Eq. (4)). Error bars represent ± 1 S.ED. of the mean estimated from binomial distribution (S.E. $= (P^*(1-P)/n)^{1/2}$, $n = 125$ trials for each condition). $^*P < 0.05$; $^{**}P < 0.005$; $^{***}P < 0.0005$.

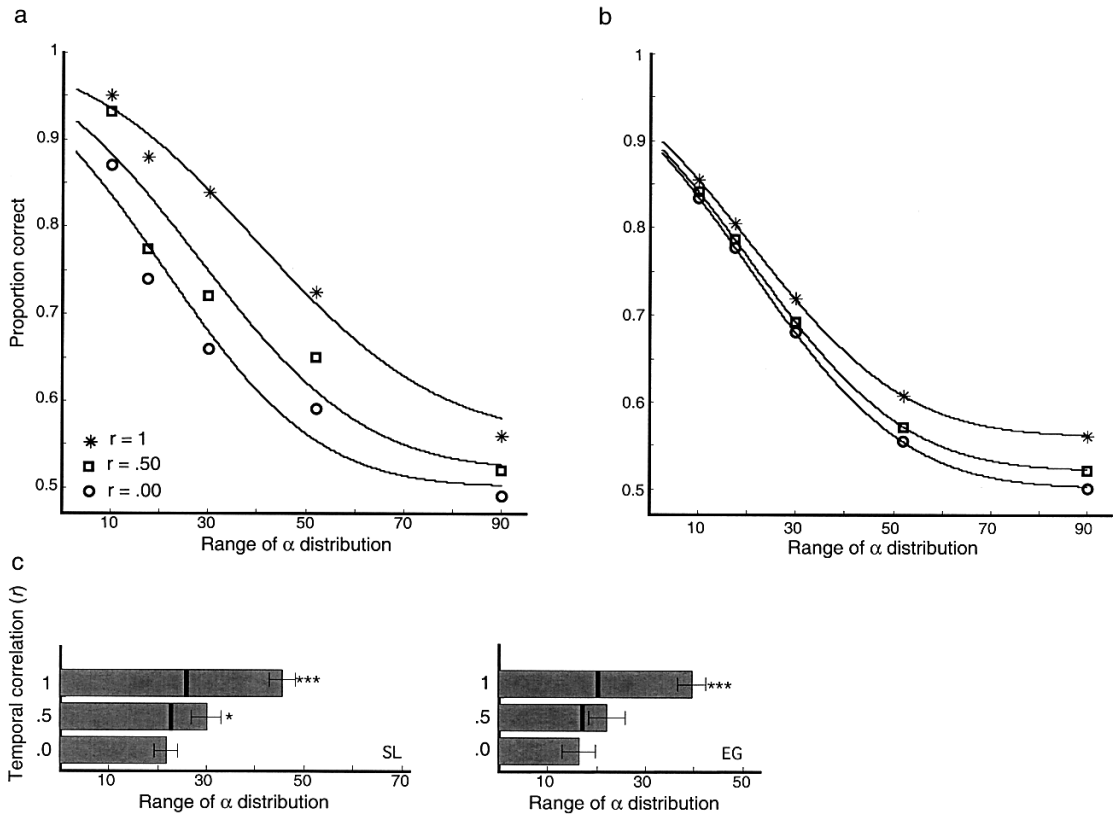

Fig. 4. Results from experiment 2. Details are the same as for Fig. 2 except that only three values of temporal correlation were tested and the temporal structure in the animation displays was now carried by changes in contrast.

alignment. Temporally correlated visual input cannot always promote visual grouping. For temporal correlation to be effective in connecting local visual features, it seems that built-in neural connections are required among neural populations that encode those local features. Taken together, by plausibly linking the efficacy of temporal structure to underlying neural circuitry, our findings provide a compelling account of results from earlier studies showing an influence of temporal factors on visual grouping (Ramachandran & Rogers-Ramachandran, 1991; Leonards, Singer, & Fahle, 1996; Usher & Donnelly, 1998).

Finally, it should be stressed that temporal structure of the sort used here is extrinsic in origin, being induced by events contained in the optical input to vision. Thus our results do not bear critically on the issue of the role of internal temporal synchrony in feature binding (Singer & Gray, 1995; Shadlen & Newsome, 1998; Gray, 1999; Shadlen & Movshon, 1999). The spatio–temporal interactions implicated in our study could be mediated by correlated modulations in firing rate or by synchronization in the temporal fine structure of action potentials. Whatever the underlying mechanism, our results underscore the inextricable link between spatial and temporal structure in vision. Our dynamic visual environment is spatially structured, and we, as observers, are constantly moving our eyes and bodies as we explore our world visually. Consequently, the optical input to vision jointly contains rich spatio-temporal structure that, in principle, can be exploited by vision for grouping and figure/ground segmentation (Conde, Macknik, & Hubel, 2000). Our findings indicate that spatial and temporal structure interact synergistically to specify features belonging to the same objects, with this synergy possibly being mediated relatively early in visual processing.

Acknowledgements

Supported by grants from the National Institutes of Health (EY07760 and EY01826).

References

Adelson, E. H., & Farid, H. (1999). Filtering reveals form in temporally structured displays. *Science*, *286*, 2231.

Alais, D., Blake, R., & Lee, S.-H. (1998). Visual features that vary together over time group together over space. *Nature Neuroscience*, *1*, 160–164.

Beck, J. (1983). Textural segmentation, second-order statistics and textural elements. *Biological Cybernetics*, *48*, 125–130.

Bosking, W. H., Zhang, Y., Schofield, B., & Fitzpatrick, D. (1997). Orientation selectivity and the arrangement of horizontal connections in tree shrew striate cortex. *Journal of Neuroscience*, *17*, 2112–2127.

Brainard, D. H. (1997). The psychophysical toolbox. *Spatial Vision*, *10*, 443–446.

Conde, S. M., Macknik, S. L., & Hubel, D. H. (2000). Microsaccadic eye movements and firing of single cells in the striate cortext of macaque monkeys. *Nature Neuroscience*, *3*, 251–258.

Das, A., & Gilbert, C. D. (1995). Long-range horizontal connections and their role in cortical reorganization revealed by optical recording of cat primary visual cortex. *Nature*, *375*, 780–784.

De Valois, R. L., & De Valois, K. K. (1991). Vernier acuity with stationary moving Gabors. *Vision Research*, *31*, 1619–1626.

Efron, B., & Tibshirani, R. (1986). Bootstrap confidence intervals and bootstrap approximations. *The Journal of the American Statistical Association*, *82*, 163–170.

Efron, B., & Tibshirani, R. (1993). *An introduction to the bootstrap*. New York: Chapman and Hall.

Fahle, M., & Koch, C. (1995). Spatial displacment, but not temporal synchrony, destorys figural binding. *Vision Research*, *35*, 491–494.

Field, D. J., Hayes, A., & Hess, R. F. (1993). Contour integrations by the human visual system: evidence for a local association field. *Vision Research*, *33*, 173–193.

Gepshtein, S., & Kubory, M. (2000). The emergence of visual objetcs in space-time. *Proceedings of the Natural Academy of Sciences*, *97*, 8186–8189.

Gilbert, C. (1993). Circuitry, architecture and functional dynamics of visual cortex. *Cerebral Cortex*, *3*, 373–386.

Graham, N. (1989). *Visual pattern analyzers*. New York: Oxford University Press.

Gray, C. M. (1999). The temporal correlation hypothesis of visual feature integration: still alive and well. *Neuron*, *24*, 31–47.

Grossberg, S., & Mingolla, F. (1985). Neural dynamics of perceptual grouping: textures, boundaries, and emergent segmentations. *Perception and Psychophysics*, *38*, 141–171.

Hess, R. F., & Dakin, S. C. (1997). Absence of contour linking in peripheral vision. *Nature*, *390*, 602–604.

Hayes, A. (2000). Apparent position governs contour–element binding by the visual system. *Proceedings of the Royal Society of London B*, *267*, 1341–1345.

Kellman, P. J., & Shipley, T. F. (1991). A theory of visual interpolation in object perception. *Cognitive Psychology*, *23*, 141–221.

Kiper, D. C., Gegenfurtuer, K. R., & Movshon, J. A. (1996). Cortical oscillatory responses do not affect visual segmentation. *Vision Research*, *36*, 539–544.

Koffka, K. (1935). *Principles of gestalt psychology*. NewYork: Harcourt Brace Jovanovich.

Kovacs, I., & Julesz, B. (1993). A closed curve is much more than an incomplete one: effect of closure on figure-ground segmentation. *Proceedings of the National Academy of Science*, *90*, 7495–7497.

Lamme, V. A. F. (1995). The neurophysiology of figure/ground segregation in primary visual cortex. *Journal of Neuroscience*, *15*, 1605–1615.

Lee, S.-H., & Blake, R. (1999a). Visual form created solely from temporal structure. *Science*, *284*, 1165–1168.

Lee, S.-H., & Blake, R. (1999b). Reply to Adelson and Farid. *Science*, *286*, 2231.

Leonards, U., Singer, W., & Fahle, M. (1996). The influence of temporal phase differences on texture segmentation. *Vision Research*, *36*, 2689–2697.

Ramachandran, V. S., & Rogers-Ramachandran, D. C. (1991). Phantom contours: a new class of visual patterns that selectively activates the magnocellular pathway in man. *Bulletin of the Psychonomic Society*, *29*, 391–394.

Regan, D., & Hamstra, S. J. (1992). Dissociation of orientation discrimination from form detection for motion-defined bars and luminance-defined bars: effects of dot lifetime and presentation duration. *Vision Research*, *32*, 1655–1666.

Roelfsema, P. R., Scholte, H. S., & Spekreijse, H. (1999). Temporal constraints on the grouping of contour segments into spatially extended objects. *Vision Research*, *39*, 1509–1529.

Schmidt, K. E., Kim, D.-S., Singer, W., Bonhoeffer, T., & Löwel, S. (1997). Functional specificity of long-range intrinsic and interhemispheric connections in the visual cortex of strabismic cats. *The Journal of Neuroscience*, *17*(14), 5480–5492.

Shadlen, M., & Movshon, J. A. (1999). Synchrony unbound: a critical evaluation of the temporal binding hypothesis. *Neuron*, *24*, 67–77.

Shadlen, M. N., & Newsome, W. T. (1998). The variable discharge of cortical neurons: implications for connectivity, computation, and information coding. *The Journal of Neuroscience*, *18*, 3870–3896.

Singer, W., & Gray, C. M.. (1995). The influence of temporal phase differences on texture segmentation. *Vision Research*, *36*, 2689–2697.

Usher, M., & Donnelly, N. (1998). Visual synchrony affects binding and segmentation in perception. *Nature*, *394*, 179–182.